Proceedings of ASME Turbo Expo 2014: Turbine Technical Conference and Exposition
GT2014
June 16 – 20, 2014, Düsseldorf, Germany

GT2014-25366

TEST RESULTS AND ANALYTICAL PREDICTIONS FOR MIL-STD-167 VIBRATION TESTING OF A DIRECT DRIVE COMPRESSOR SUPPORTED ON AMB

Lawrence A. Hawkins
Calnetix Technologies
Cerritos, California, USA

Rasish K. Khatri
Calnetix Technologies
Cerritos, California, USA

Koman B. Nambiar
YORK® Navy Systems,
Johnson Controls
York, Pennsylvania, USA

ABSTRACT

External vibration testing was performed on a semi-hermetic, direct drive compressor on magnetic bearings intended for US Navy Shipboard use. The compressor was placed on a US Navy MIL-STD-167 shaker platform and driven at sinusoidal frequencies from 4 to 33 Hz at graduated displacements equal to a maximum of 1.5Gs. During the machine design phase, a linear forced response analysis of the coupled rotordynamic system model of the rotor, housing and magnetic bearings was performed to predict rotor/housing displacements and actuator loads. The results were used to guide bearing sizing and control algorithm design. The measured rotor motion and actuator currents correlated well with predictions at all tested frequencies, amplitudes and orientations. Analysis methodology, test results, and comparisons are reported here.

INTRODUCTION

Successful operation has been demonstrated for a developmental prototype compressor for a new generation of shipboard chillers for the U.S. Navy. Chillers provide vital cooling for ship weapons, command and control systems, and crew comfort. These chillers must be designed for 35 to 50 years of service during which they will be exposed to extreme environments such as weapons-effect shock, heavy-weather ship vibration, and temperatures ranging from the Arctic to tropical locations. The new high efficiency small-capacity (HES-C) chiller was developed to improve shipboard heating, ventilating and air conditioning (HVAC) systems by significantly increasing cooling density and reliability while decreasing fuel consumption and maintenance.

The new HES-C chillers are based on variable speed economized two-stage compressors with active magnetic bearings (AMB) and a high-speed permanent magnet motor. Full speed, full power testing of the new HES-C compressor has demonstrated that all of the Navy's aggressive goals will be achieved. The chillers are slated for new ship design and construction. The compressor has also been designed as a retrofit option to improve the performance and energy usage of more than 200 chillers already in fleet use. Construction of production units is expected to commence in 2014 with the first ship installation scheduled in 2015.

In addition to system-level testing up to full speed and full power of the developmental prototype, the compressor in stand-still (0 rpm shaft speed) was tested separately for its ability to meet Navy MIL-STD-167 vibration and MIL-S-901D shock testing requirements. This was accomplished as risk-mitigation to the operational vibration and heavy weight shock qualification that is expected to be completed in 2015 for the first HES-C production chiller. The sensitivity of the crew places a natural limit on ship vibration levels. However, the Navy's MIL-STD-167 vibration testing is formulated to assess two categories of vibration failure: (1) insufficient stiffness or clearance in the design, and (2) mechanical fatigue, either by breakage or general loosening of major structural elements or nonstructural components, such as switch contacts or component lead wires. Both failure categories are sensitive to the amplitude of the vibration stimulus, though they differ in that failures of the first category may never occur at reduced vibration levels, while failures of the second category merely take longer to appear. For the first category, amplitude-sensitive failures, the MIL-STD-167 variable-frequency test applies an input-amplitude greater than is expected in the field, and the item under test is observed for any undue response. For the second category, the MIL-STD-167 endurance test simulates fatigue failure by raising the input amplitude to the

point where the item under test will receive, in a few hours, the same fatigue it would receive at lower vibration levels after many years on the ship.

For vibration testing, the compressor was placed on a shaker platform driven at sinusoidal frequencies from 4 to 33 Hz at up to 1.5Gs (Fig. 1). The excitation was applied in the radial and axial directions both separately and simultaneously. For the vibration testing, these requirements had to be met at stand-still without backup bearing contact. A base motion analysis was developed to ensure that the final design would meet the requirements. The predicted load capacity needed to meet the vibration requirement was a significant fraction of the overall load capacity requirement for the magnetic bearings in all directions. The measured rotor motion correlated well with analytical predictions at all tested frequencies, amplitudes, and load orientations. The analysis approach is described here along with a comparison of measurements and predictions. A future paper will revisit the analysis after the vibration test of the operating HES-C chiller, expected in 2015.

Figure 1. HES-C Compressor Mounted on the Shaker Table.

For shock testing, the compressor in stand-still was placed on a Navy-Approved Medium Weight Shock Machine and exposed to a graduated series of shock loads ending with a pulse exceeding 50Gs, as measured at the compressor housing. The auxiliary bearings, specially designed to carry the shock load, met all expectations. The results of this testing will be reported in a future paper.

SYSTEM MODEL

The compressor discussed here is based on a high speed permanent magnet synchronous motor with a five-axis magnetic bearing system and two integral centrifugal impellers – one on each end of the machine. The two radial bearings are homopolar, permanent magnet-bias bearings with design load capacity of 3,122 N (700 lb_f) each. Actuator negative stiffness is 6,150 N/mm (35,000 lb_f/in) for each radial bearing. The design characteristics for this type of bearing have been previously discussed by Filatov [1]. For easy reference in this document, the non-thrust end radial bearing, shown in Fig. 2, is often referred to as Brg 1, and the thrust end radial bearing is often referred to as Brg 2. The axial bearing is an electromagnetic bias bearing with design load capacity of 6,244 N (1400 lb_f) and a negative stiffness of 7,125 N/mm (40,000 lb_f /in). The magnetic bearing system was sized to accommodate the rotor weight of 103 kg (227 lb_m), aerodynamic loads, transient unbalance loads, ship motion and inclination, and the loads imposed by the MIL-STD-167 vibration requirements.

The backup bearing system for each end of the machine consists of a duplex, face/face pair of angular-contact ball bearings in a compliant mount. The backup bearings are a typical configuration with steel races, a full complement of ceramic balls, no cage, and grease film lubrication. The total axial clearance between the backup bearing inner ring and the shaft thrust faces is 0.356 mm (0.014 in). The radial clearance between the backup bearing inner ring and the shaft is 0.18 mm (0.007 in). In addition to the usual functions of supporting the rotor during non-operation of the AMB and for process overload of the AMB, the backup bearings in this machine are also required to provide the primary support for shock loads. The system must withstand a 50 G shock at the machine supports and remain functional. This requirement was the key driver for the sizing of the backup bearings.

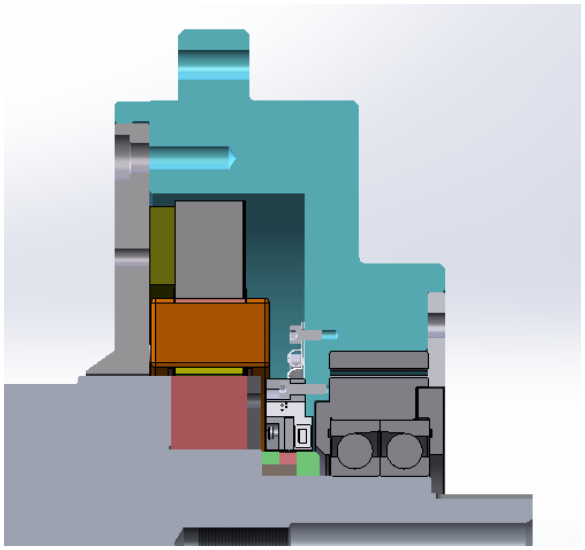

Figure 2. General Assy. of Radial Bearing 1 (non-thrust end).

A rotor/housing/magnetic bearing system model was created to develop the initial stabilizing magnetic bearing compensator as well as to analyze the behavior of the compressor on the shaker table. This system model, shown in Fig. 3, includes a rotor structural dynamic model, a simple housing structural dynamic model, and a magnetic bearing model representing the important dynamics of the magnetic bearing system. The rotor is modeled using standard industry practice – a stiffness model using beam elements that include shear deflection terms, and a lumped mass model. The impellers are represented by lumped inertias at nodes coinciding with their respective centers-of-

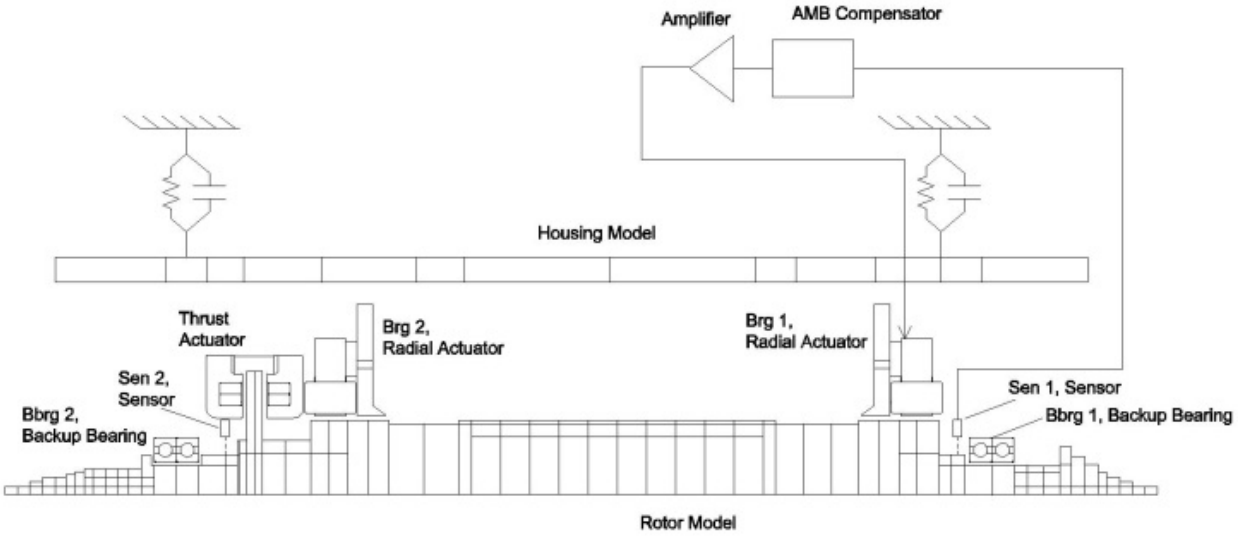

Figure 3. Rotor/Housing/Magnetic Bearing System Model.

gravity. The housing model is relatively simple, but it adequately represents the mass distribution and provides nodes to attach supports and excitation forces for both the external vibration analysis and control algorithm development. The housing is connected to ground with two springs and dampers to produce a lowest natural frequency of 5 Hz and damping ratio of 12.5%.

The rotordynamic equation of motion for the compressor, which is in general a coupled, flexible rotor/housing system, is:

$$\begin{bmatrix} M_R & 0 \\ 0 & M_C \end{bmatrix} \begin{Bmatrix} \ddot{q}_R \\ \ddot{q}_C \end{Bmatrix} + \begin{bmatrix} D_R + G_R & 0 \\ 0 & D_C \end{bmatrix} \begin{Bmatrix} \dot{q}_R \\ \dot{q}_C \end{Bmatrix} + \begin{bmatrix} K_R & 0 \\ 0 & K_C \end{bmatrix} \begin{Bmatrix} q_R \\ q_C \end{Bmatrix} = \begin{Bmatrix} f_{mb,R} \\ f_{mb,C} \end{Bmatrix} + \begin{Bmatrix} f_{ext,R} \\ f_{ext,C} \end{Bmatrix} \quad (1)$$

Or

$$M\ddot{q} + D\dot{q} + Kq + K_{act}q = f_{mb} + f_{ext} \quad (2)$$

where the subscripts R and C refer to rotor and housing (casing) structures, M, D and K are the mass, damping and stiffness matrices, respectively, for the separate rotor and housing structures, G_R is the gyroscopic matrix containing skew symmetric products of polar inertia and spin speed, K_{act} is a sparse matrix containing entries for the passive actuator negative stiffness, q is the physical displacement vector, f_{mb} is a vector containing the control forces from the magnetic bearing actuators, and vector f_{ext} contains external forces such as unbalance forces on the rotor or external vibration inputs into the housing. In machines where there are additional fluid or aerodynamic elements, conventional rotordynamic coefficients can be added to Eq. (2) as necessary.

For system analysis with magnetic bearings, the compressor represented by Eq. (2) is converted to state space form:

$$\begin{bmatrix} \dot{q} \\ \ddot{q} \end{bmatrix} = \begin{bmatrix} 0 & I \\ -M^{-1}(K + K_{act}) & -M^{-1}D \end{bmatrix} \begin{bmatrix} q \\ \dot{q} \end{bmatrix} + \begin{bmatrix} 0 \\ M^{-1}B_S^* \end{bmatrix} u_{mb} + \begin{bmatrix} 0 \\ M^{-1} \end{bmatrix} f_{ext} \quad (3)$$

Or

$$\begin{aligned} \dot{x}_S &= A_S x_S + B_{S,act} u_{mb} + B_{S,ext} f_{ext} \\ y_{sen} &= C_{S,sen} x_S \\ y_{rel} &= C_{S,rel} x_S \end{aligned} \quad (4)$$

where the subscript S designates the combined structural dynamic models, u_{mb} is a vector of actuator forces and has one row for each actuator, B_S* is a selection matrix to connect the actuator forces to the correct rotor and housing degrees-of-freedom, $C_{S,sen}$ is a selection matrix to retrieve the relative rotor/housing position sensor signals y_{sen} for connection to the magnetic bearing transfer model, and $C_{S,rel}$ is a selection matrix to retrieve relative rotor/housing position and velocity for points of interest. More complete steps for this process are available in [2], albeit with different notation.

The magnetic bearing force/displacement transfer functions are conveniently represented in state space form:

$$\begin{aligned} \dot{x}_{mb} &= A_{mb} x_{mb} + B_{mb}\, y_{sen} \\ u_{mb} &= C_{mb}\, x_{mb} \end{aligned} \quad (5)$$

Where B_{mb} connects the sensor inputs to the magnetic bearing controller and C_{mb} retrieves the actuator forces. This magnetic bearing model includes the compensator (control algorithm) plus the sensor, anti-aliasing filter, amplifier, actuator dynamics, and calculation and conversion time delays. The magnetic bearing force/displacement transfer functions developed for this system are shown in Figure 4 for Brg 1, Brg

2, and the axial bearing. These transfer functions can be represented in state space form by Eq. (5). For the system analysis, this magnetic bearing model is coupled to the structural dynamic model as follows:

$$\begin{Bmatrix} \dot{x}_S \\ \dot{x}_{mb} \end{Bmatrix} = \begin{bmatrix} A_S & B_{S,act}C_{mb} \\ B_{mb}C_{S,sen} & A_{mb} \end{bmatrix} \begin{Bmatrix} x_S \\ x_{mb} \end{Bmatrix} + \begin{bmatrix} B_{S,ext} & 0 \\ 0 & 0 \end{bmatrix} \begin{Bmatrix} f_{ext} \\ 0 \end{Bmatrix}$$

$$\begin{Bmatrix} y_S \\ u_{mb} \end{Bmatrix} = \begin{bmatrix} C_{S,rel} & 0 \\ 0 & C_{mb} \end{bmatrix} \begin{Bmatrix} x_S \\ x_{mb} \end{Bmatrix} \quad (6)$$

Or

$$\dot{x}_{sys} = A_{sys}x_{sys} + B_{sys,ext}\, f_{ext}$$
$$y = C_{sys}x_{sys} \quad (7)$$

where for stability analysis, the f_{ext} is set to zero and the eigenvalues of the system matrix, A_{sys}, are calculated. For this forced response analysis, the Laplace transform is applied to Eq. (7), yielding:

$$X_{sys}(s)\left(sI - A_{sys}\right) = B_{sys,ext}\, F_{ext}(s) \quad (8)$$

At each analysis frequency, the known excitation forces are loaded into the force vector and Eq. (8) is solved for the states X_{sys}. Rotor and housing displacements and magnetic bearing control forces can be retrieved from X_{sys} using the output description in Eq. (6).

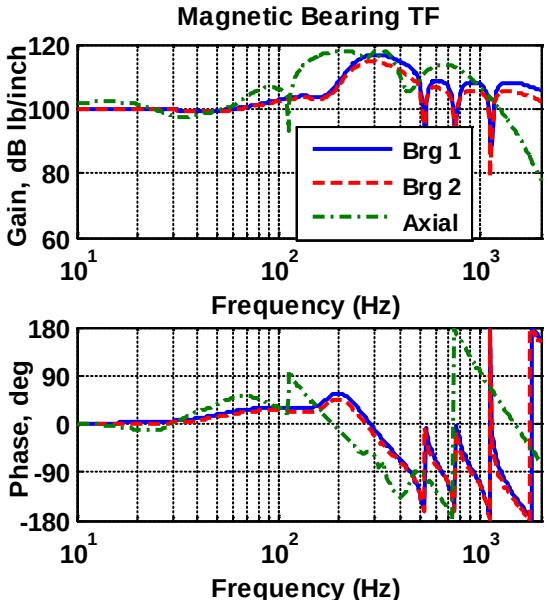

Figure 4. Magnetic bearing force/displacement transfer functions for Brg 1, Brg 2, and axial bearing.

EXTERNAL VIBRATION ANALYSIS (MIL-STD-167)

External Vibration Requirements

The compressor was designed to meet modified Type I vibration requirements in accordance with MIL-STD-167-1A under vibration conditions of 4 to 25 Hz. Additional exploratory testing was performed up to 33 Hz. The total frequency range is divided into three sub ranges with a different vibration amplitude requirement for each sub range. The required amplitudes have a tolerance so the worst-case values, given in Table 1, were used for the design requirement. When tested, the vibration is imposed by placing the compressor on a shaker table and stepping through the frequency ranges in 1 Hz increments. This is a base vibration of fixed amplitude so the worst-case condition for each frequency range occurs at the highest frequency in the range (10, 15 and 25 Hz) since that is where the maximum acceleration occurs.

Table 1. Magnetic Bearing Vibration Test per Modified MIL-STD-167-1A

Frequency Hz	Max 0 - pk Displacement (inch)	Acceleration at highest frequency	
		Max in/sec^2	Max g's
4 to 10	0.150	592	1.53
11 to 15	0.036	320	0.83
16 to 25	0.024	592	1.53

If the magnetic bearings could be made stiff enough such that the lowest natural frequency is well above the excitation frequency, then the rotor motion would closely approximate the housing motion. In this case, the additional load capacity needed to meet the vibration requirements would simply be the apparent rotor weight associated with the maximum acceleration from Table 1. For example, with the base vibration of 0.150 inch at 10 Hz, the two radial bearings would together share a load of 1.53 times the shaft weight during the vertical shake tests, and the axial bearing would need to react an additional load of 1.53 times shaft weight during the horizontal (axial) shake test. However, there is a constraint on using a very stiff magnetic bearing as the effect of sensor noise becomes less manageable as compensator gain is increased. Thus, when the housing is being shaken there will be some relative rotor/housing displacement. Even so, the magnetic bearings must be stiff enough such that the relative rotor/housing displacement is less than the backup bearing clearance with some design margin. There is another reason to limit the relative displacement – the load capacity of the actuator drops when the rotor moves away from the actuator center, so increased motion results in the need for additional load capacity. In effect, the negative stiffness of the actuator imposes an additional load penalty since the load capacity

drops by roughly the product of the offset from magnetic center times the negative stiffness.

In essence this means that when sizing the actuator, additional load capacity is needed to accommodate both the shaft acceleration and to account for the lost load capacity from being off center. The best way to determine this required additional capacity is to simply perform a base vibration analysis of the complete rotor/housing/magnetic bearing system under the required conditions.

Eq. (8) can be solved for the system response to an excitation force imposed on the housing; however, the required displacements versus frequency are prescribed by Table 1 and the force required to achieve that for this system is unknown. There are several ways to determine the necessary force – one choice is to calculate a dynamic flexibility matrix at each analysis frequency using Eq. (8):

$$V_{flex}(s) = \left(sI - A_{sys}\right)^{-1} \tag{9}$$

Then, assuming an applied force at node i corresponding to the axial location of the housing center of gravity, use Eqs. (8) and (9) to determine the force to achieve the desired displacement at the housing center of gravity:

$$F_{ext}(j\omega) = \frac{X_{sys}(j\omega)_i}{V_{flex}(j\omega)_{i,i}\, B_{sys,ext}} \tag{10}$$

So at each analysis frequency, ω, the prescribed displacement from Table 1 is used in Eq. (10) to determine the required excitation force at that frequency. This force is then used in Eq. (8) to determine the complete system response such as the rotor/housing displacements at locations of interest, coil currents, and magnetic bearing forces. Another way to accomplish this goal is to run a trial frequency response analysis using a constant amplitude excitation force. Then the results can be used to scale the excitation force to achieve the desired housing vibration, and this force is used in a subsequent frequency response run. Both methods will give the same result.

The results of the analysis are shown in Figs. 5, 6, and 7. Figure 5 shows the predicted absolute housing displacement at the two magnetic bearing sensor locations. The displacement is a near match to the prescribed values in Table 1. The discrepancy occurs because the rotor CG doesn't exactly coincide with the housing CG. An exact match could be achieved by using two forces and two displacements with Eq. (10). Figure 6 shows the relative rotor/housing displacements at the actuator, sensor, and backup bearing associated with Bearing 2. Bearing 2 results are shown because the displacements and loads are marginally higher than at Bearing 1. There are three peaks in the curve corresponding to the highest frequency for the three different housing excitation amplitudes. The response is considerably lower at 15 Hz than 10 Hz because the associated acceleration is lower. The overall peak displacement at the backup bearing is 0.0032 inch occurring at 25 Hz. This is about 50% of the backup bearing clearance, well within the requirement of no contact. Figure 7 shows the Bearing 2 actuator force versus frequency. There are three curves:

1) $\mathbf{F}_{control}$ – the actuator force, $\mathbf{u}_{mb}$ from Eq. (6), is the force produced by the control flux,
2) $\mathbf{F}_{negative}$ – the decentering force due to the actuator negative stiffness, and
3) $\mathbf{F}_{net}$ – the resultant force on the rotor at the actuator, this is the vector sum of $\mathbf{F}_{control}$ and $\mathbf{F}_{negative}$.

At any given frequency, $\mathbf{F}_{negative}$ is simply the actuator relative displacement times the actuator negative stiffness. Even though $\mathbf{F}_{net}$ is the net force delivered to the rotor, the magnetic bearing system actuators, amplifiers and power supply must be sized to deliver the force $\mathbf{F}_{control}$ for the purposes of meeting the requirements from Table 1. Of course, the load capacity requirements defined here are only one of several load elements contributing to the overall magnetic bearing system sizing.

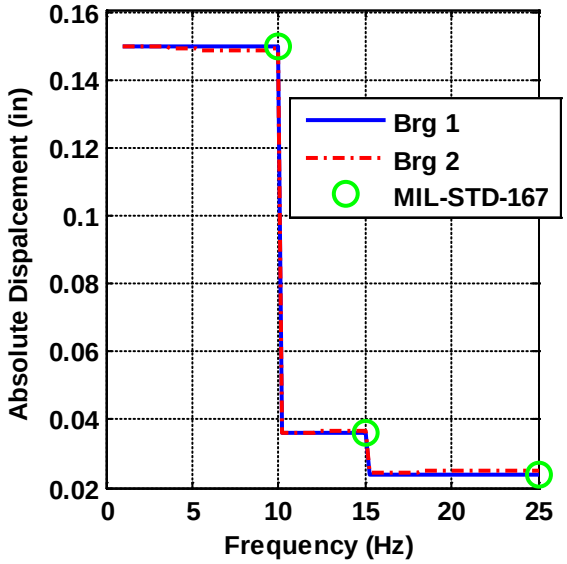

Figure 5. Nominal housing absolute displacement due to frequency dependent excitation force per MIL-STD-167.

Because of the impact on actuator sizing, the rotor/housing relative displacement from this analysis was used as a performance measure in the control compensator development. Limiting the peak of the sensitivity transfer function was the other [4]. As expected, increasing the compensator gain reduces rotor/housing motion and thus the required actuator force, $\mathbf{F}_{control}$.

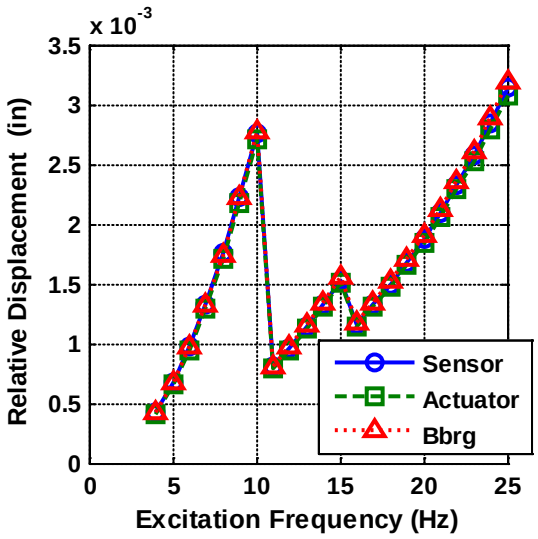

Figure 6. Predicted Bearing 2 rotor/housing relative displacements due to MIL-STD-167 frequency dependent excitation force.

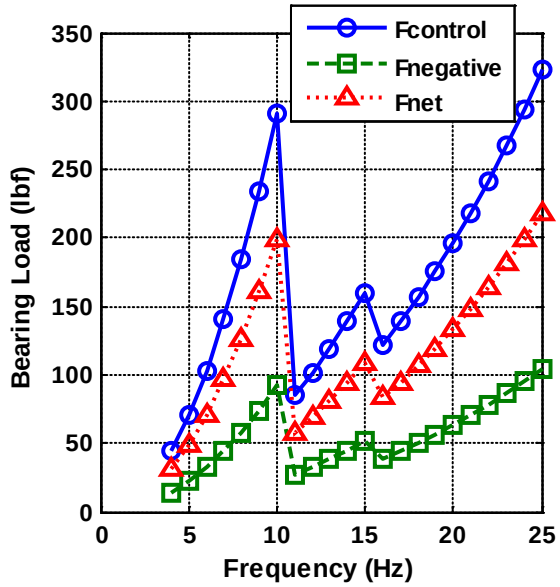

Figure 7. Predicted Bearing 2 reaction loads due to MIL-STD-167 frequency dependent excitation force.

COMPARISON OF SHAKER TABLE MEASUREMENTS TO ANALYSIS

The vibration testing was conducted at an independent test lab on an inertial shaker table that used counter-rotating shafts with eccentric weights phased to create a sinusoidal force along a fixed axis, either vertical or horizontal (Fig. 1). The speed of the motor driving the shafts was varied to vary excitation frequency, and the eccentricity of the weights adjusted to vary the unbalance and therefore excitation force and table displacement. The machine was placed on the shaker table as shown in Fig. 1. Vertical excitation was used to test the radial bearings. As the bearing poles (axes) are orientated at 45° to the vertical, all radial control axes are reacting load in this situation. Horizontal vibration, along the shaft axis, was used to test the axial bearings. Finally, the machine was tested at a 30° incline using an incline fixture, to load all five axes simultaneously. The excitation was applied for 1 minute at each test frequency except at 25 Hz, when the excitation was applied for 60 minutes to evaluate thermal performance.

Acceptance Criteria

The acceptance criteria for the vibration portion of the test include:

1) The magnetic bearings must maintain stable rotor levitation throughout each test.
2) Magnetic Bearing Controller (MBC) ambient temperature must not exceed 60°C (140°F) throughout each test.
3) MBC amplifier temperatures must not exceed 95°C (203°F) throughout each test.
4) The HES-C compressor must maintain structural and electrical integrity throughout each test.

Vibration Testing Results

Figures 8-13 show the predicted and measured results of the vibration testing. Data measured during the tests include: housing accelerations at each bearing location and at the shaker table in the excitation direction, position sensor displacement and commanded current for all five magnetic bearing control axes, actuator temperatures, and MBC amplifier and ambient temperatures. The housing acceleration data was taken manually from the vibration monitors at the start of each excitation. The rotor displacement and current command data for all five axes were sampled from the MBC at 5 kHz using a high-speed data acquisition system. For each excitation frequency, the average amplitude at the excitation frequency over the five minute excitation period (30 minutes for 10 Hz) was used to represent the sensor displacement and current at each frequency. Measured actuator control load is calculated from the measured current command data by multiplying by the known amplifier transfer function and by the actuator transfer function. For the radial measurements shown, the bandwidth of the actuator is well above the maximum excitation frequency so the transfer function is essentially constant and equal to the actuator gain in lb_f/amp or N/amp. For the axial excitation, the actuator transfer function was calculated using a magnetic FEA and updated based on a measurement of the compressor axial plant transfer function. The Brg 1 and Brg 2 load measurements represent the vector sum of the X and Y axis loads calculated from X and Y axis current command data as just described.

Figure 8 is a plot of the absolute housing vibration at the two ends of the compressor during the frequency sweep, along with

the value used for the design analysis (the Table 1 values). It is clear that the excitation level from 4-10 Hz was well below the design specification. This was due to the displacement limitation of the shaker table at the independent test lab. The Navy deemed this acceptable since the highest loads are expected at the 25 Hz frequency along with the greatest power demands from the MBC.

Another shortcoming of the test data is the difference in the displacement at the two ends of the machine. The intended purely vertical motion would produce identical displacements at the two ends. The difference could be due to a number of things: 1) the center-of-gravity of the compressor was not in line with the force axis of the shaker table, 2) flexibility of the housing foot-to-table mounting was different on the two ends of the compressor, and 3) incorrect calibration of the housing accelerometers used to quantify base motion. The percent difference between the two measurements is about 6% with a total difference of about 0.003 inch (± 0.0015 inch) in the frequency range between 15 and 25 Hz. For the predicted results shown below, the measured housing motions of Figure 8 are taken at face value and used to create the forcing function for the analysis.

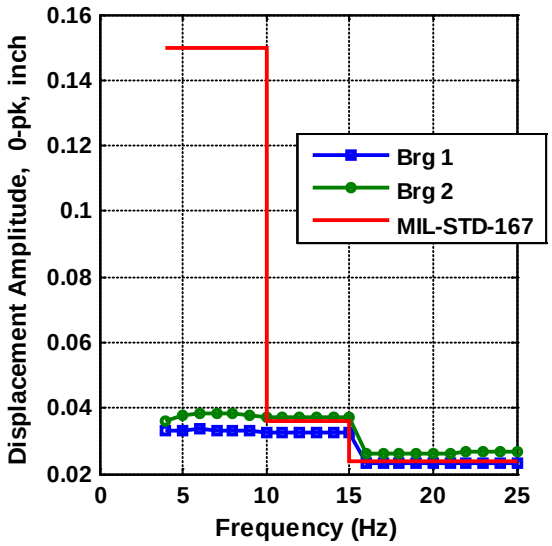

Figure 8. Measured housing vibration during shaker table testing.

Figures 9-11 show predicted and measured frequency response results. The predictions shown here are calculated using the same method described in the design analysis, but they are updated to use the measured housing vibration of Fig. 8. Figures 9 and 10 show predicted and measured relative displacement at the Brg 1 and Brg 2 sensors, respectively. Since the vibration was vertical and between the two poles of the bearing, the measured displacement is the vector sum of the X and Y position sensor measurements and predictions. The maximum measured displacement, 0.0034 inch, occurs at Brg 2 at 25 Hz. There is a missing measurement point at 13 Hz because the test was stopped at this point to make an adjustment in the shaker table. When the test was restarted, the high frequency data collection was not restarted in time to collect the 13 Hz point.

The relative displacement predictions in Figures 9 and 10 correlate very well with the measurements, but the Brg 1 relative displacement is slightly over-predicted by the model and the error is growing roughly linearly with frequency. The authors attribute this largely to discrepancies between the actual versus measured base motion of Figure 8. This topic is discussed in more depth in the next section.

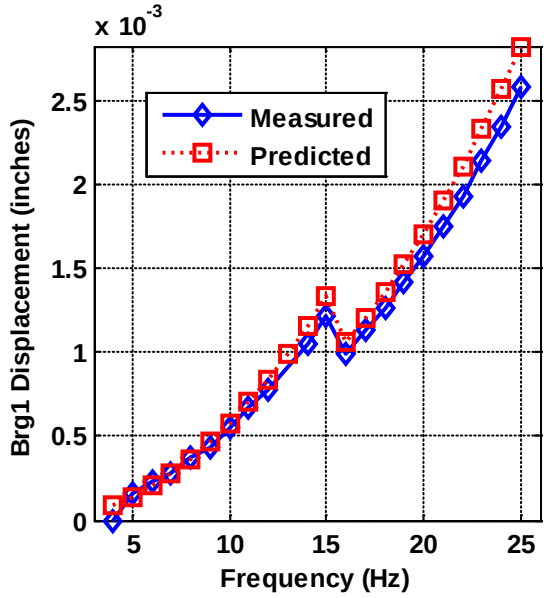

Figure 9. Measured and predicted rel. rotor/housing displacement at Brg 1 position sensors using measured housing vibration as input.

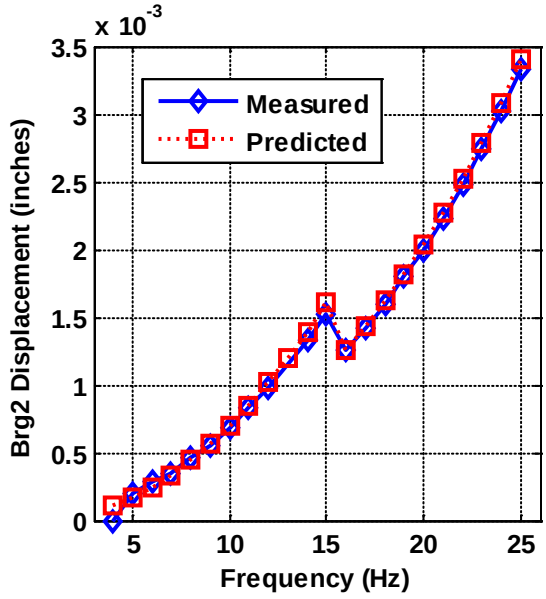

Figure 10. Measured and predicted rel rotor/housing displacement at Brg 2 position sensors using measured housing vibration as input.

Figure 11 shows the predicted actuator reaction force along with the experimental actuator reaction force for both radial bearings. The predicted actuator force is $\mathbf{F}_{control}$ and the measured reaction force is calculated from the measured control current. The predicted Brg 2 values in Fig. 11 are equivalent to the predicted $\mathbf{F}_{control}$ values in Fig. 7 with the adjustment for measured housing vibration. There is a small systematic discrepancy in predicted and measured force for Brg 1, but this can be attributed to the same mechanism as the error in Figure 9.

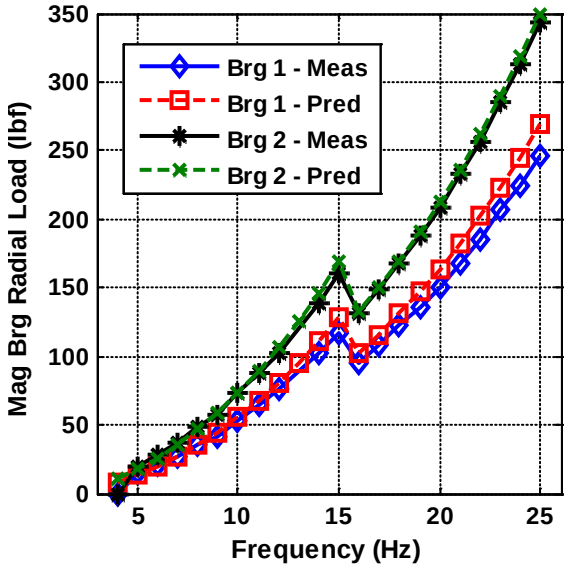

Figure 11. Measured and predicted net loads at Brg 1 and Brg 2 using measured housing vibration as input.

Figures 12 and 13 show predicted and measured frequency response results for the axial vibration acceptance test. The predicted displacement and bearing loads are well-predicted by the model. There is a small discrepancy between the measurements and predictions that is apparent at the higher frequencies. The trend follows a similar pattern to the radial Brg 1 results. The maximum steady-state displacements and bearing loads are under 0.006 inch and 600 lb_f as expected during the design analysis. A comparison of Figs. 12 and 13 to Figs. 9-11 shows that the response rises much more rapidly with frequency in the axial direction than in the radial direction. This result is seen in both the measurement and analysis. This phenomenon is caused by the low actuator bandwidth of the axial channel. This could be counteracted by changes to the control compensator, but at the expense of poorer noise performance due to increased gain in the compensator. The worst-case condition for the axial acceptance test occurs at 25 Hz, as expected.

Uncertainty Discussion

Several sources of uncertainty were considered to explain the small but systematic discrepancy found between the

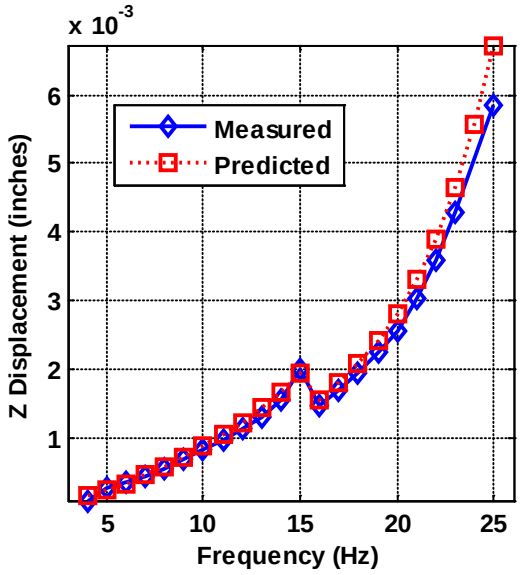

Figure 12. Measured and predicted relative rotor/housing displacement at axial sensors using measured housing vibration as input.

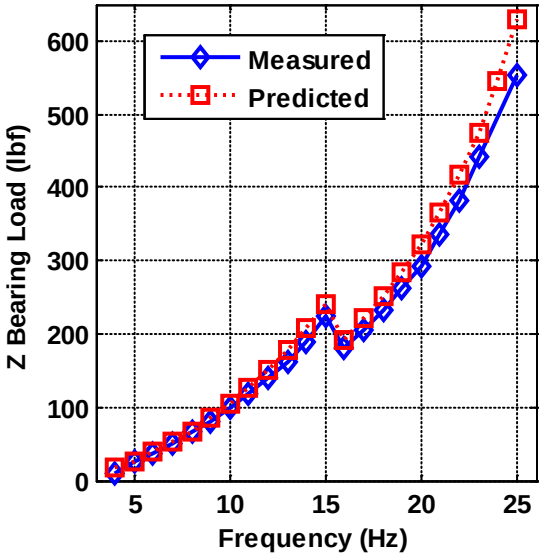

Figure 13. Measured and predicted actuator force at the thrust bearing using measured housing vibration as input.

measurements and predictions for Brg 1 (Figures 9 and 11) and the axial bearing (Figures 12 and 13).

1.) If the basic linear model closed loop frequency response were not a good match to the small signal frequency response of the actual system then the model-to-prediction discrepancies reported here could result. The radial and axial models do match well so this is an unlikely source of the error. Of course, unmodeled amplitude dependent non-linear

characteristics could cause the observed discrepancies since the response amplitudes are increasing with frequency.

2.) The calibrated magnetic bearing position sensor uncertainties are ±3.5% radial and ±4.0% axial. However, the linearity is very good in this displacement range and the frequencies of interest are far below the sensor bandwidth.

3.) A constant magnetic bearing negative stiffness value was used in the model, whereas, negative stiffness generally becomes larger with displacement. However, the permanent magnet bias actuator used here has nearly constant negative stiffness at up to twice the tested displacements. Further, if the model included a negative stiffness that increased with amplitude, the new predicted displacement would be larger and thus would not explain the discrepancy in Figure 9.

4.) The measured base motions from Figure 8 are a possible source of error as discussed earlier. To get an estimate of the effect of a base motion measurement error, an uncertainty of 0.0015 inch (50% of the difference between Brg 1 and Brg 2 displacements) was assigned to the Figure 8 values and the analysis repeated for the two extremes. The results, shown in Figure 14 for Brg 1, indicate that if the actual base motion was 0.0015 inch lower than measured, then the predicted relative displacement would match well versus frequency.

The two most likely causes of the small model to measurement discrepancies found at higher frequencies are: (1) unmodeled non-linear effects and (2) error in the measurement of the base (housing) motion at the actuators. As discussed above, the known non-linear effects should be small. Imperfect knowledge of the base motion is a prime candidate, given the size of the machine and test platform.

SUMMARY AND CONCLUSIONS

Stand-still vibration testing has been completed for a new direct drive compressor on magnetic bearings intended for US Navy Shipboard use. During the design phase of the machine, a numerical analysis approach was established to predict the additional magnetic bearing load capacity needed to meet the vibration requirements imposed by Navy MIL-STD-167. The analysis was described and results presented and discussed. In addition to including rotordynamic structural models for the rotor and housing, the analysis included the key dynamics of the magnetic bearing system: sensor and anti-aliasing filter, compensator, calculation and conversion time delays, amplifier, and actuator. It was shown that the magnetic bearing must be sized for both: (1) the load needed to move the rotor along with the housing, and (2) to replace the lost load capacity from relative rotor/housing motion. The compressor was direct coupled to a shaker table and driven at sinusoidal frequencies from 4 to 33 Hz at graduated displacements equal to a maximum of 1.5Gs. The analysis and test results indicated excellent convergence. A small discrepancy appeared at the higher frequencies. Possible sources of this discrepancy were discussed.

This first stand-still vibration testing suggests that the Navy's goal of a conservative, robust design will be realized as the stand-still testing was accomplished at vibration displacements and frequencies that exceed the operational chiller requirements. In future testing, the entire chiller will be placed on a shaker table and operated at full speed and power. The coupling of the compressor to the chiller shell will present dynamic differences that will allow further refinement of the algorithms which will be reported in a future paper.

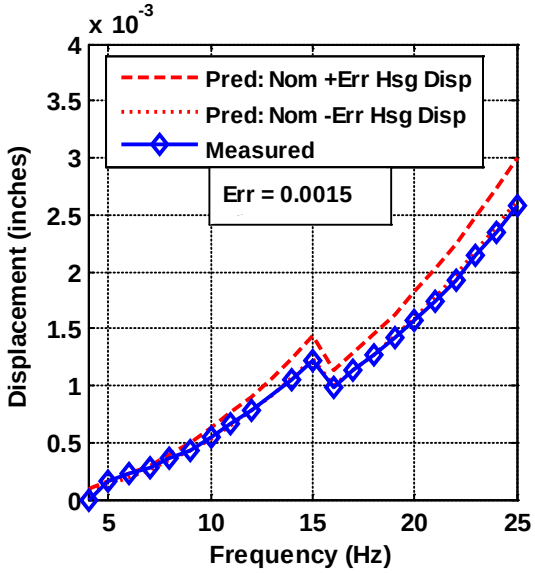

Figure 14. Predicted Brg 1 relative displacement, using nominal +Err and nominal –Err (Err = 0.0015 inch) base motion, compared to measured relative displacements.

ACKNOWLEDGEMENT

The work reported here was supported by the American Recovery and Reinvestment Act (ARRA) of 2009, through U.S. Navy Contract N65540-06-D-0021, Program Manager: Neil Antin; Naval Sea Systems Command, Washington, DC. The United States Government retains, and by accepting the article for publication, the publisher acknowledges that the United States Government retains, a non-exclusive, paid-up, irrevocable, worldwide license to publish or reproduce the published form of this work, or allow others to do so, for United States Government purposes.

REFERENCES

[1] Filatov, A.V., McMullen, P.T., Hawkins, L.A. Blumber, E., 2004, "Magnetic Bearing Actuator Design for a Gas Expander Generator," *Proc. 9th Intl. Symp. on Magnetic Bearings*, Lexington, Kentucky, USA.

[2] Schweitzer, G., Maslen, E.H, 2009, *Magnetic Bearings: Theory, Design, and Application to Rotating Machinery*, Springer Verlag, Berlin, Germany, pp. 288-294.

[3] Hawkins, L.A., Murphy, B.T., Zierer, J., Hayes, R., 2002, "Shock and Vibration Testing of an AMB Supported Energy Storage Flywheel", *Proc. 8th Int. Symp. on Magnetic Bearings*, Mito, Japan.

[4] ISO, 2006, *Mechanical vibration – Vibration of rotating machinery equipped with active magnetic bearings – Part 3: Evaluation of stability margin*, 14839-3:2006, International Organization for Standardization, Geneva, Switzerland.